Color Glass Condensate approach to Heavy Ion Collisions

藤井宏次

- **x-evolution for HIC**
- **Glasma instability – N.O. type**

Ref. 板倉数記、物理学会誌５９巻３号
Gelis-Lappi-Venugopalan, 0708.0047
Iancu-Venugopalan, hep-ph/0303204
Iancu-Leonidov-McLerran, hep-ph/0202270

Evidences of CGC:

Geometric Scaling

Stasto, Geloc-Bienat, Kwiecinski
PRL 86 (2001) 596

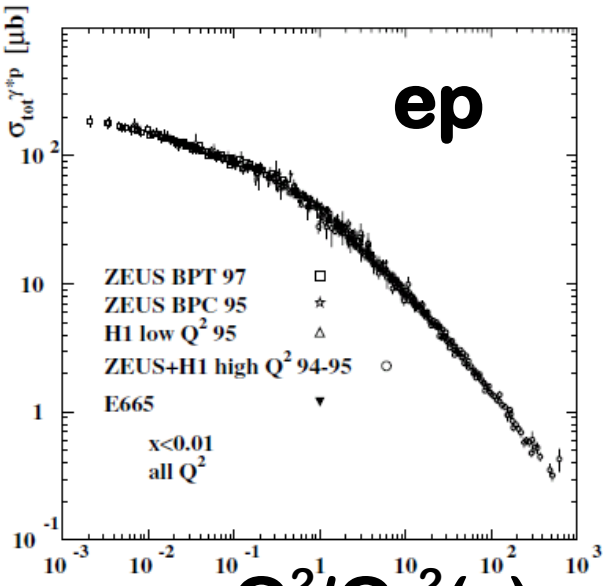

FIG. 1. Experimental data on $\sigma_{\gamma^* p}$ from the region $x < 0.01$ plotted versus the scaling variable $\tau = Q^2 R_0^2(x)$.

Freund, Rummukainen, Weigert, Schafer
PRL 90 (2003) 222002

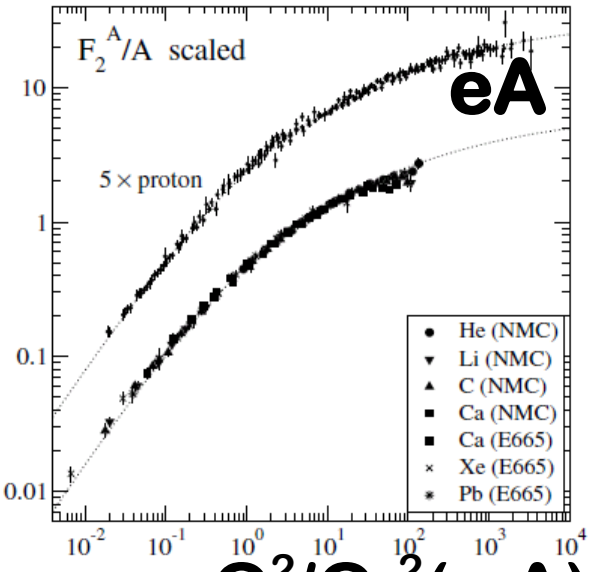

FIG. 3. Scaling behavior of NMC and E665 F_2^A data vs $\tau = (\frac{x_N}{x_0})^{2\lambda} \frac{Q^2}{A^{1/3}}$. The vertical axis corresponds to the left-hand side of Eq. (5). The dashed line corresponds to the geometric scaling curve obtained from HERA data. These are shown offset by a factor of 5.

Marquet, Schoeffel
Phys.Lett. B639 (2006) 471

Diffractive ep

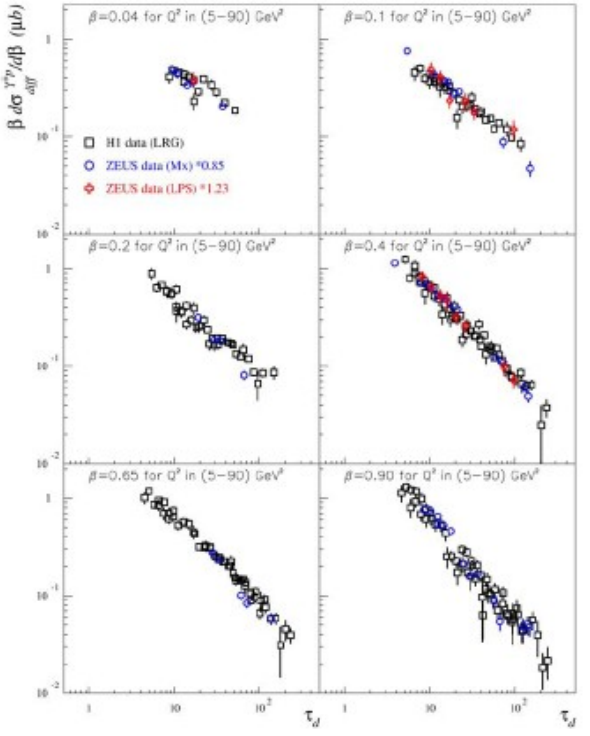

Fig. 2. The diffractive cross-section $\beta d\sigma_{\rm diff}^{\gamma^* p \to Xp}/d\beta$ from H1 and ZEUS measurements, as a function of τ_d in bins of β for Q^2 values in the range [5; 90] GeV^2 and for $x_{\rm P} < 0.01$. Only statistical uncertainties are shown.

スケールの存在； $Q_s^2(x) \sim A^{1/3} (1/x)^{0.3}$

Small x

x ~ M / sqrt(s) ~ 0.01 (RHIC), ~0.0005(LHC)

大きな輻射補正 --> 足し上げ

重イオン衝突での"物質生成"に重要な領域

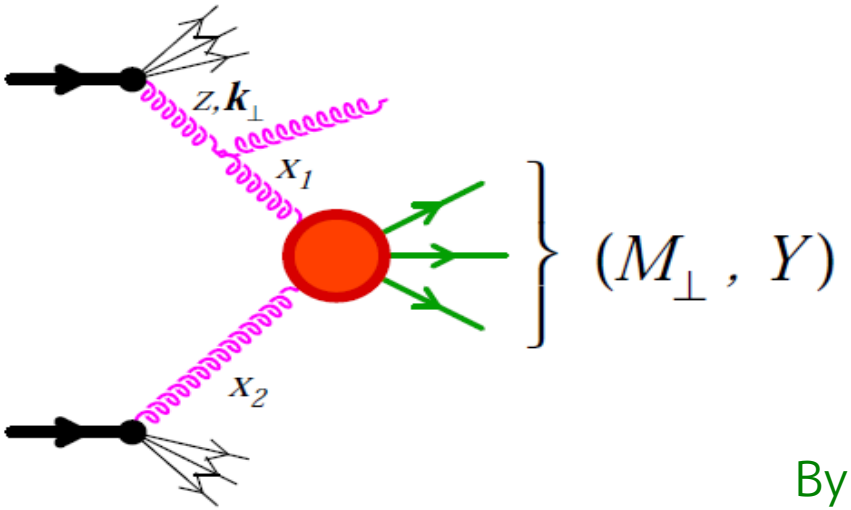

By Gelis

$$\alpha_s \int_{x_1} \frac{dz}{z} \int^{M_T} \frac{d^2 k_T}{k_T^2} \sim \alpha_s \log(1/x_1) \log(M_T)$$

Onium scattering; BK (BFKL)

アイコナール近似振幅； エネルギー依存無し

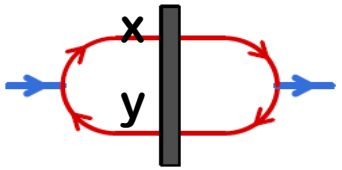

$$= \left|\Psi^{(0)}(\boldsymbol{x}_\perp, \boldsymbol{y}_\perp)\right|^2 \mathrm{tr}\left[U(\boldsymbol{x}_\perp)U^\dagger(\boldsymbol{y}_\perp)\right]$$

Balitsky, Mueller,
Kovner-Wiedemann
Gelis et al.

ブーストによって見える揺らぎ

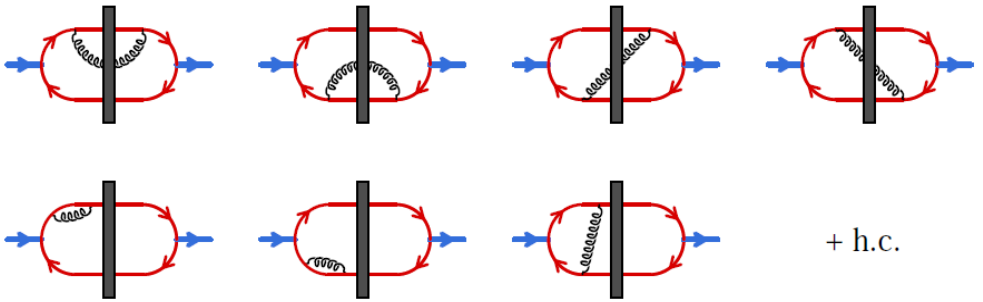

$$\frac{\partial \boldsymbol{S}(\boldsymbol{x}_\perp, \boldsymbol{y}_\perp)}{\partial Y} = -\frac{\alpha_s N_c}{2\pi^2}\int d^2\boldsymbol{z}_\perp \frac{(\boldsymbol{x}_\perp - \boldsymbol{y}_\perp)^2}{(\boldsymbol{x}_\perp - \boldsymbol{z}_\perp)^2(\boldsymbol{y}_\perp - \boldsymbol{z}_\perp)^2} \times\left\{\boldsymbol{S}(\boldsymbol{x}_\perp, \boldsymbol{y}_\perp) - \boldsymbol{S}(\boldsymbol{x}_\perp, \boldsymbol{z}_\perp)\boldsymbol{S}(\boldsymbol{z}_\perp, \boldsymbol{y}_\perp)\right\}$$

$$\boldsymbol{S}(\boldsymbol{x}_\perp, \boldsymbol{y}_\perp) \equiv \mathrm{tr}\left[U(\boldsymbol{x}_\perp)U^\dagger(\boldsymbol{y}_\perp)\right]/N \qquad Y \equiv \ln(p^+/\Lambda)$$

Onium scattering; BK (BFKL)

for T = 1 - S

$$\frac{\partial T(x_\perp, y_\perp)}{\partial Y} = \frac{\alpha_s N_c}{2\pi^2} \int d^2 z_\perp \frac{(x_\perp - y_\perp)^2}{(x_\perp - z_\perp)^2 (y_\perp - z_\perp)^2}$$
$$\times \Big\{ T(x_\perp, z_\perp) + T(z_\perp, y_\perp) - T(x_\perp, y_\perp) - T(x_\perp, z_\perp) T(z_\perp, y_\perp) \Big\}$$

- 線形項のみ＝ **BFKL**
  - **T ~ exp(λY)**
- 非線型項＝ **BK**
  - グルーオン結合・飽和
- 標的平均　**<TT> ~ <T><T>**

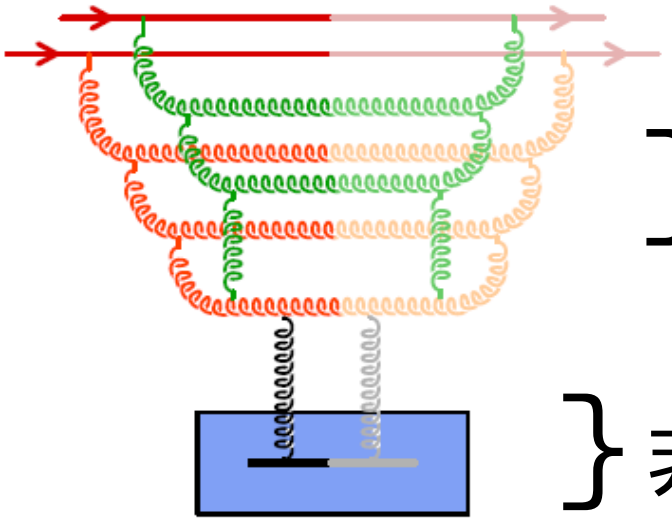

Small x

BFKL カスケードによる高密度グルーオンの生成
＋ グルーオン再結合による飽和状態の出現
==> 全てのハドロン、原子核に普遍な状態

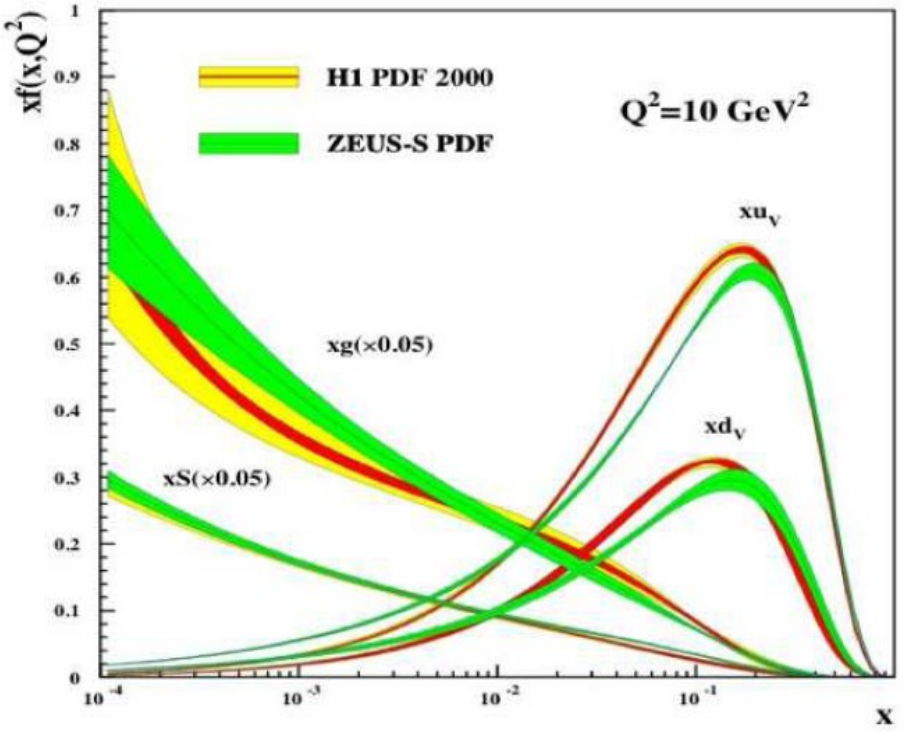

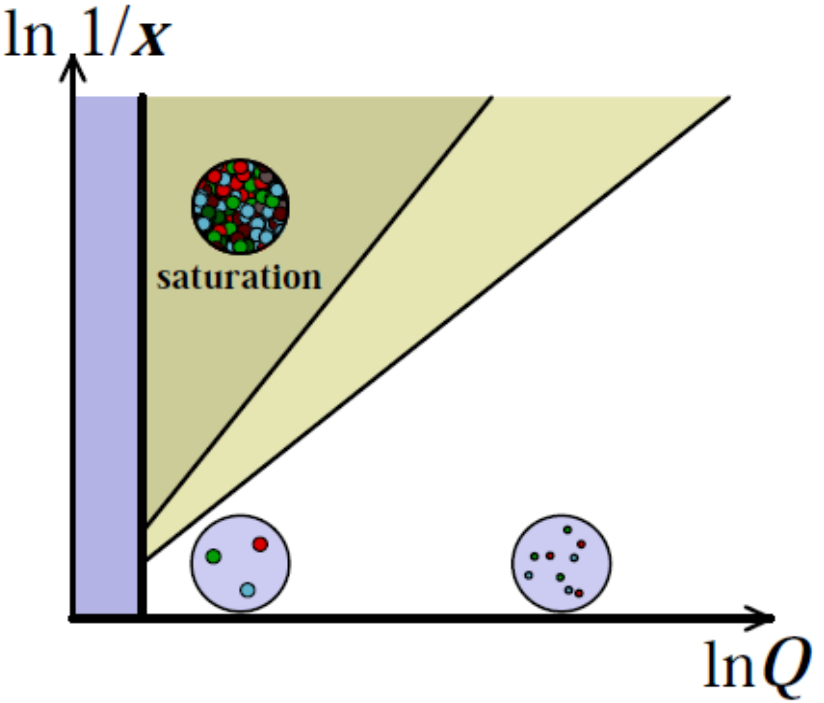

Color Glass Condensate framework

ターゲットを二つの自由度に分離して考える有効理論

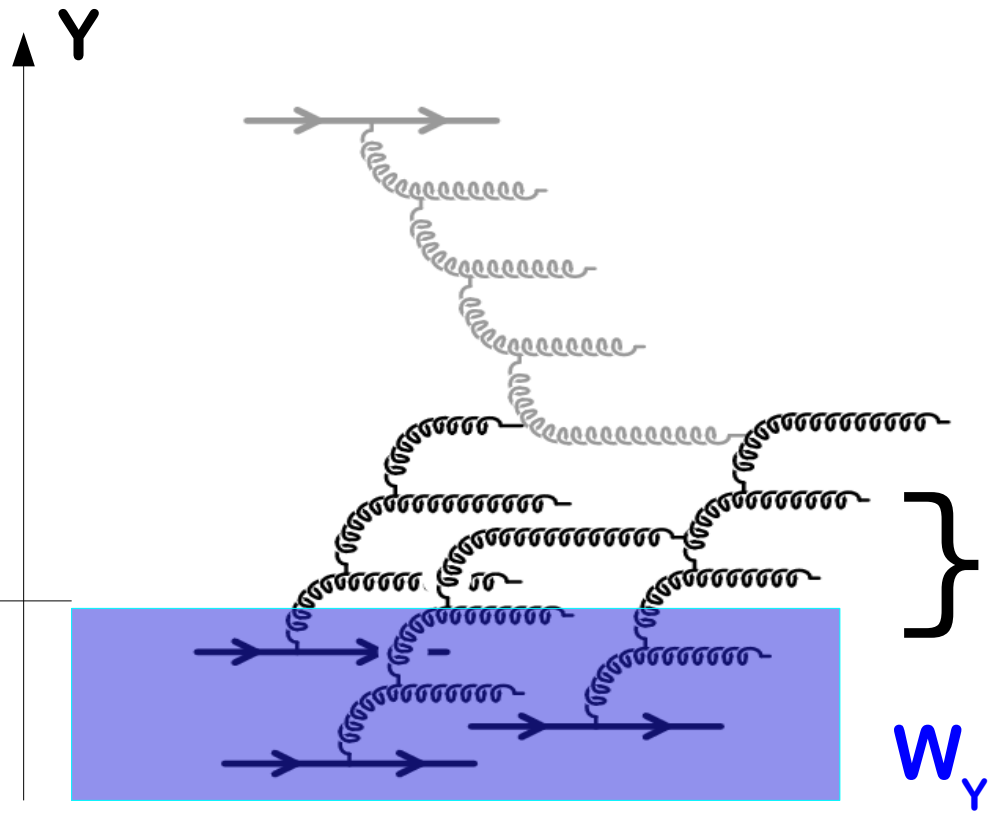

濃密だが揺動的

$Qs(y) >> \Lambda_{QCD}$

$W_Y[\rho]$; カラー荷分布（非揺動）

$W_y[\rho]$ に対するくりこみ群方程式（ **JIMWLK** ）

McLerran-Venugopalan Gaussian Model

原子核の **W** に対する模型 **(e.g., x~0.01)**

局所的ガウス分布平均

$$W = \exp\left[-\int d^2x\,\rho(x)_a^2/2\mu^2\right]$$

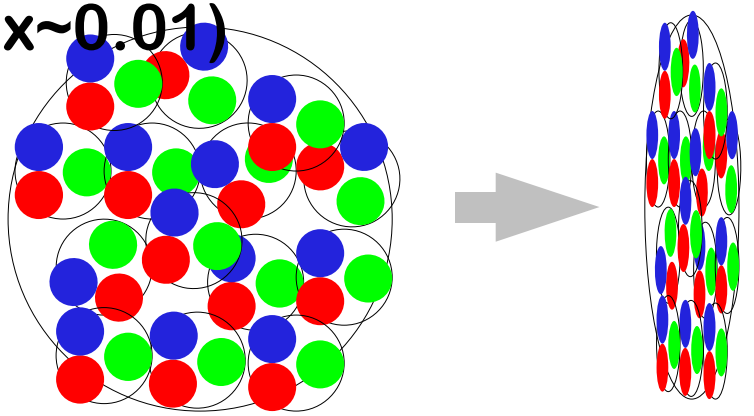

$$[D_\nu, F^{\nu\mu}]_a = \delta^{\mu+}\delta(x^-)\rho_a(\vec{x}_\perp)$$

- カラー荷面密度 $\mu^2 \sim \mu_0{}^2 A^{1/3} >> \Lambda_{QCD}{}^2$ **==>** 弱結合
- 古典解 **F** の下で物理量を評価

==> コヒーレント多重散乱効果 **$O(g^2\rho)=1$**

例：グルーオン分布

$$\begin{aligned}
\phi_A^{g,g} &\sim \boldsymbol{k}_\perp^2 \,\mathrm{FT}\,\langle U(\boldsymbol{x})\,U^\dagger(\boldsymbol{y})\rangle \\
U(\boldsymbol{x}) &\equiv \mathcal{P}\exp\left[ig^2\int dz^+(1/\nabla^2)\rho(z^+,\boldsymbol{x})\cdot T\right] \\
xg(x,Q^2) &= \frac{1}{4\pi^3}\int dk_\perp^2\,\phi_A^{g,g}(x,k_\perp^2)
\end{aligned}$$

MV Initial cond for BK evolution

- MV model at x~0.01
- scale $\mu^2 \sim Q_s^2 \sim A^{1/3}$
  - $0.22\ \mathrm{GeV}^2$ …"proton"
  - $2.0\ \mathrm{GeV}^2$ … "nucleus"
- Gluon dist w/ intrinsic kT
- $1/k^2$ – perturbative tail

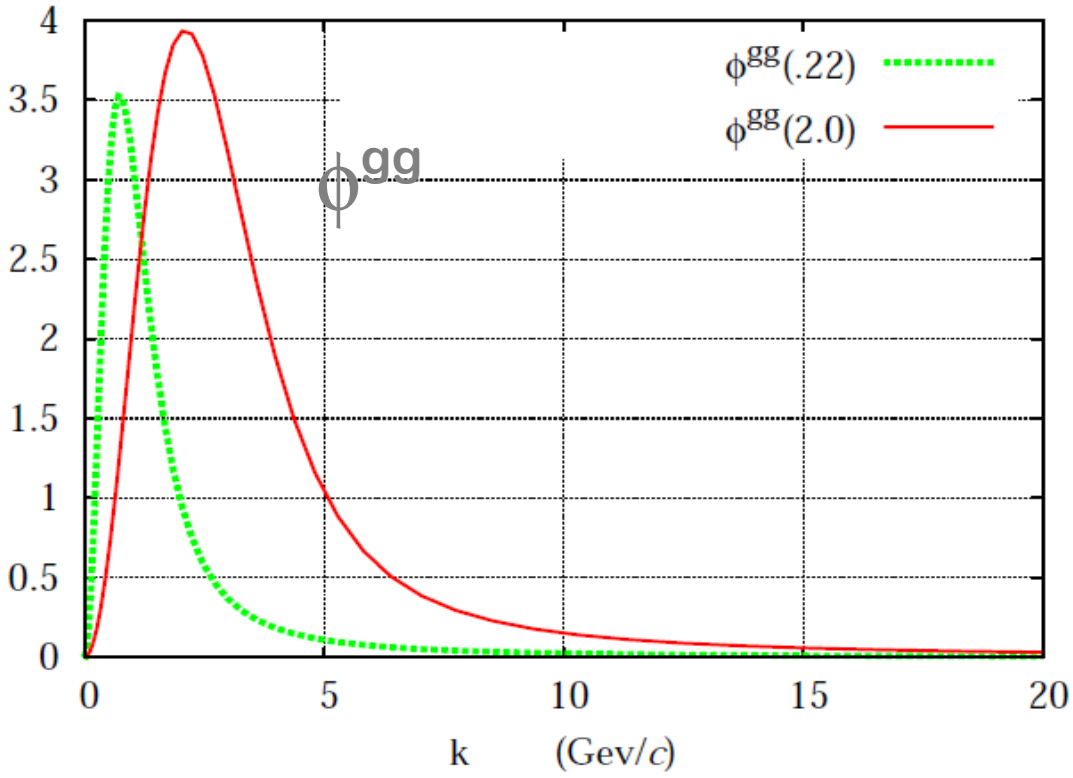

BK x-evolution

- **BK eqn w/o b-dep.**
  - **Linear: BFKL sums up (α_s y)**

    <-- 両者を分かつスケールの存在
  - **Nonlinear: gluon fusion effect**

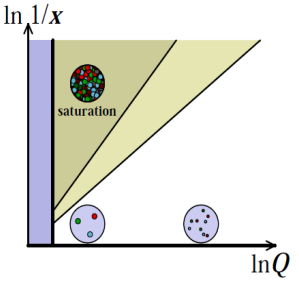

$$\frac{\partial}{\partial Y} T_Y(\boldsymbol{k}_\perp) = \bar{\alpha}_s \left[\chi(-\partial_L) T_Y(\boldsymbol{k}_\perp) - T_Y^2(\boldsymbol{k}_\perp) \right]$$

$\bar{\alpha}_s = \alpha_s N/\pi, \qquad L \equiv \ln(k_\perp^2/\Lambda^2)$

$\chi(\gamma) = 2\psi(1) - \psi(\gamma) - \psi(1-\gamma)$: BFKL kernel

$T_Y(\boldsymbol{k}_\perp) = \int \frac{d^2\boldsymbol{x}_\perp}{2\pi \boldsymbol{x}_\perp^2} (1 - \langle \widetilde{U}\widetilde{U}^\dagger \rangle) e^{i\boldsymbol{k}_\perp \cdot \boldsymbol{x}_\perp}$

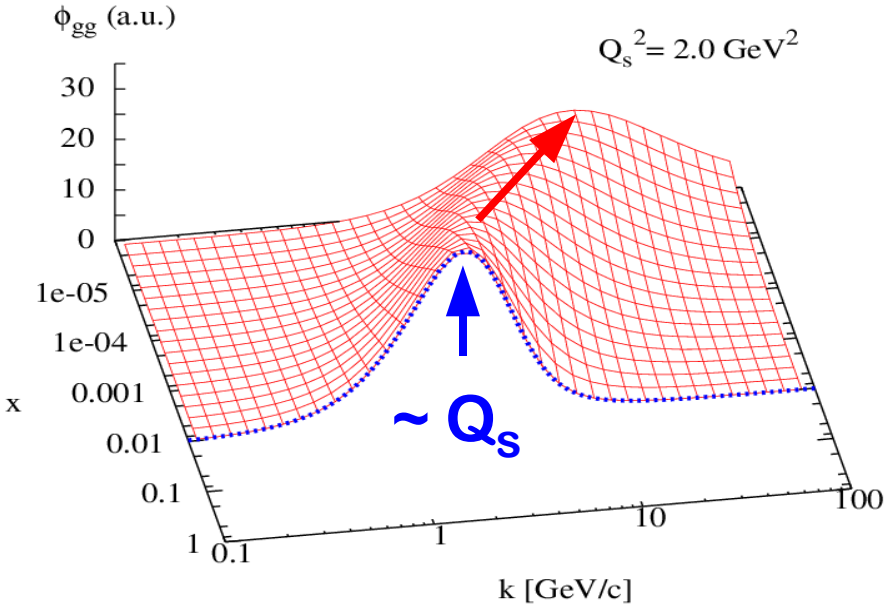

BK x-evolution

- スケール解への漸近

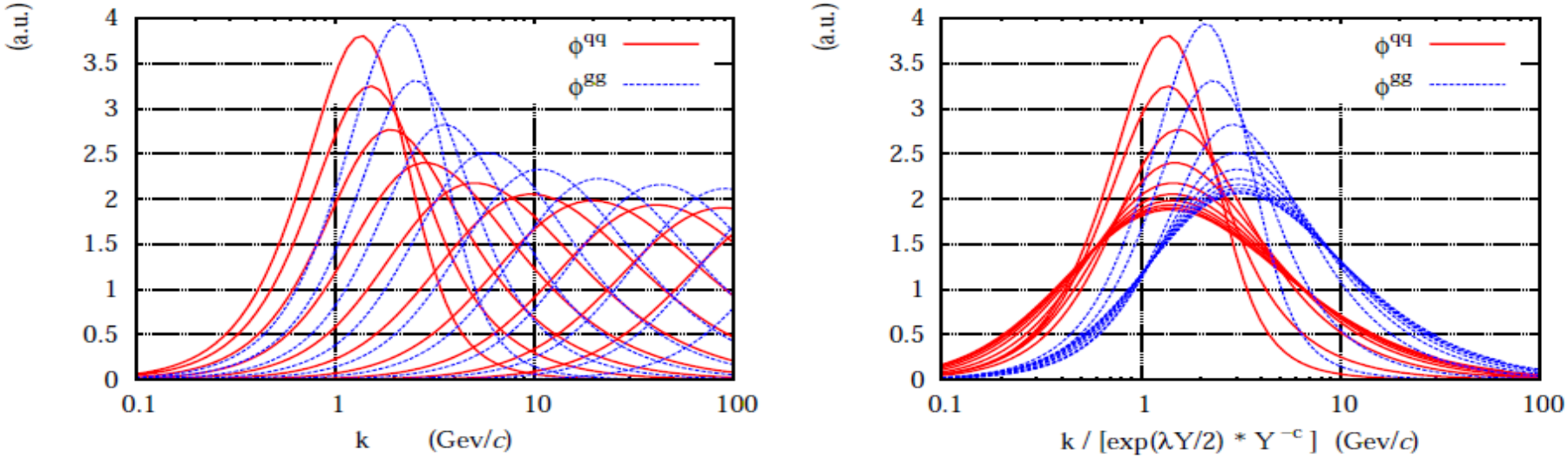

Figure 1: Numerical solution of the BK equation with an initial condition corresponding to the MV model ($x_0 = 0.01$, $Q_s^2 = 2.0$ GeV), as a function of $k_\perp$ (left: $Y - Y_0$=0, 2, 4, $\cdots$, 18) and as a function of the scaling variable $k_\perp/[e^{\lambda Y} Y^{-c}]$ (right: $Y - Y_0$=0, 2, 4, $\cdots$, 18). The coupling constant in the BK equation is set to $\alpha_s = 0.2$.

Asymptotics: Muller-Triantafyllopoulos

BK x-evolution

- **LO evolution**
  - 大きい λ
  - **Qs** 陽子 **が Qs** 核 **より早く増大**
  - 初期分布に敏感

$$Q_s^2(x,A) \sim A^{1/3} x^{-\lambda}$$

$\lambda = 4.88\,\bar{\alpha}_s$ (LO BFKL)

$\lambda \sim 0.3 \quad x = 10^{-2} - 10^{-4}$ (NLO BFKL)

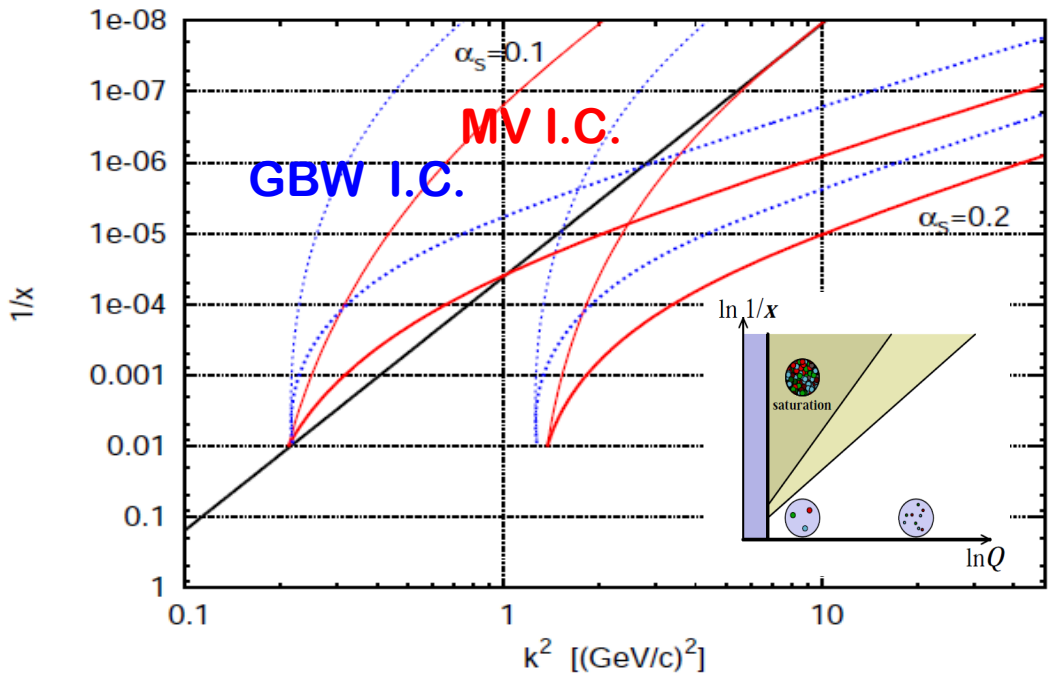

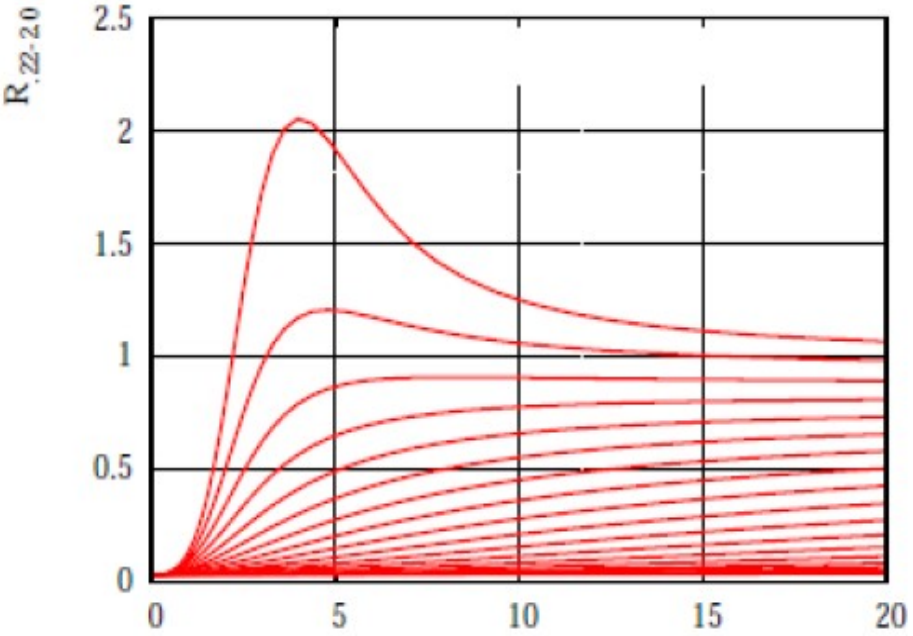

BK x-evolution

- **LO evolution**
  - 大きい λ
  - **Qs** 陽子 **が Qs** 核 **より早く増大**
  - 初期分布に敏感

$$Q_s^2(x,A) \sim A^{1/3} x^{-\lambda}$$

$\lambda = 4.88\,\bar{\alpha}_s$ (LO BFKL)

$\lambda \sim 0.3 \quad x = 10^{-2} - 10^{-4}$ (NLO BFKL)

NLO-BK available

Balitsky, Kovchegov-Weigert
Albacete-Kovchegov,
Balitsky-Chirilli

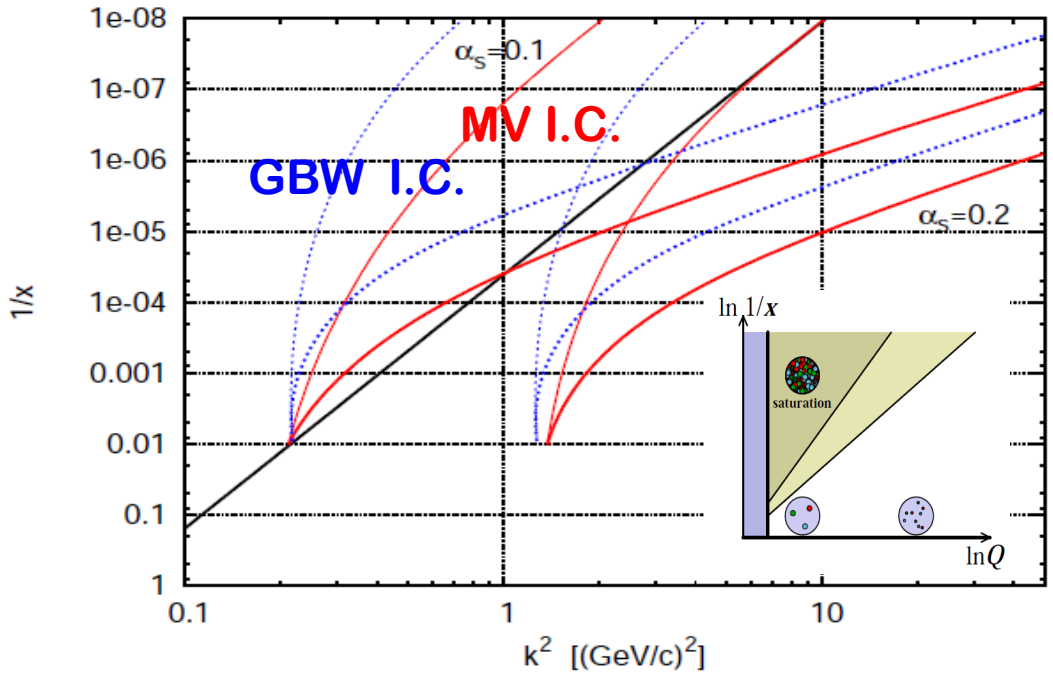

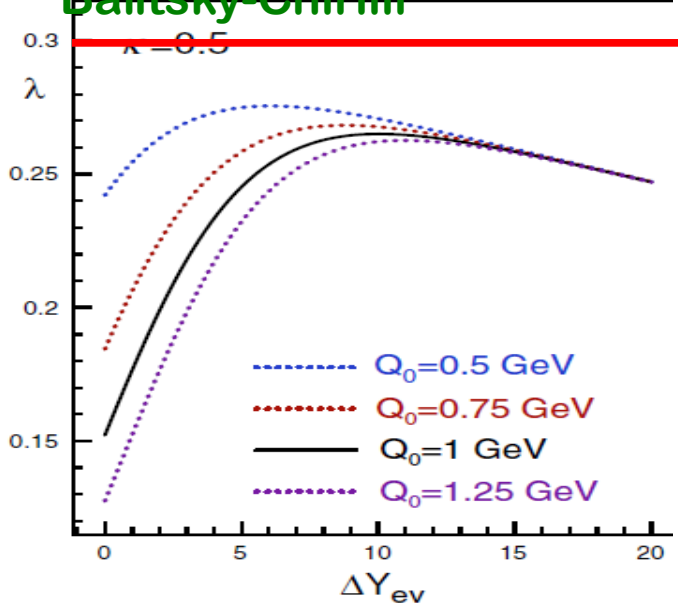

Evidences of CGC:

Geometric Scaling

Stasto, Geloc-Bienat, Kwiecinski
PRL 86 (2001) 596

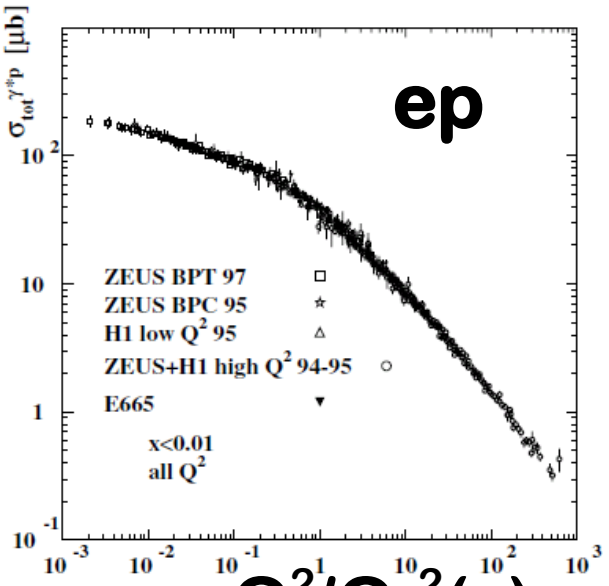

FIG. 1. Experimental data on $\sigma_{\gamma^* p}$ from the region $x < 0.01$ plotted versus the scaling variable $\tau = Q^2 R_0^2(x)$.

Freund, Rummukainen, Weigert, Schafer
PRL 90 (2003) 222002

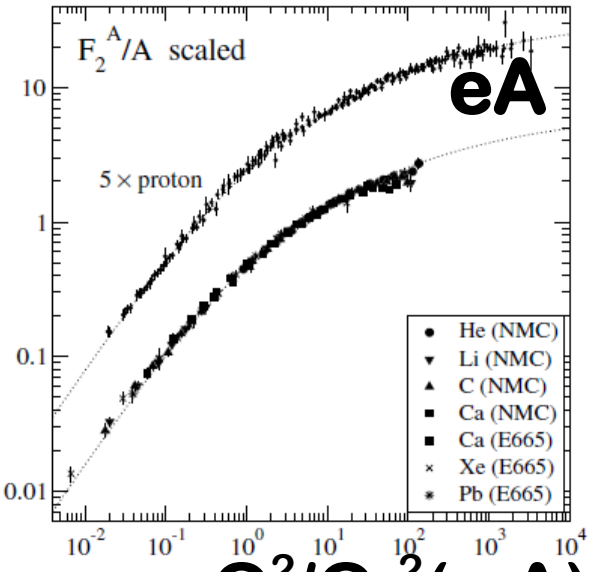

FIG. 3. Scaling behavior of NMC and E665 F_2^A data vs $\tau = (\frac{x_N}{x_0})^{2\lambda} \frac{Q^2}{A^{1/3}}$. The vertical axis corresponds to the left-hand side of Eq. (5). The dashed line corresponds to the geometric scaling curve obtained from HERA data. These are shown offset by a factor of 5.

Marquet, Schoeffel
Phys.Lett. B639 (2006) 471

Diffractive ep

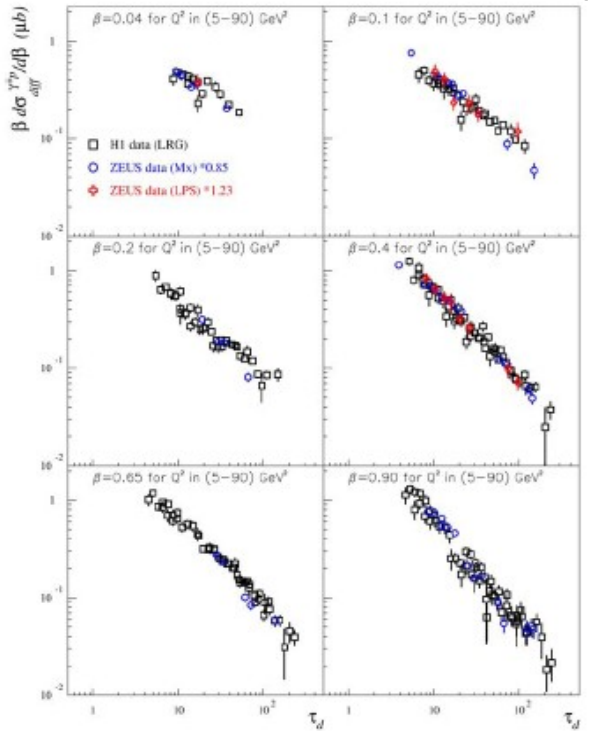

Fig. 2. The diffractive cross-section $\beta d\sigma_{\rm diff}^{\gamma^* p \to Xp}/d\beta$ from H1 and ZEUS measurements, as a function of τ_d in bins of β for Q^2 values in the range [5; 90] GeV^2 and for $x_{\rm P} < 0.01$. Only statistical uncertainties are shown.

Saturation gives the scale Qs
fixes x-, A- dependences

Implications to HIC phenomenology

- **Gluon production**
  - **Assumption: kT factorization**

$$\frac{dN_{\rm ch}}{dyd^2b} = C\frac{4\pi N_c}{N_c^2-1}\int\frac{d^2p_t}{p_t^2}\int^{p_t} d^2k_t\,\alpha_s(Q)\,\varphi\left(x_1,\frac{|\underline{k}_t+\underline{p}_t|}{2}\right)$$
$$\times\,\varphi\left(x_2,\frac{|\underline{k}_t-\underline{p}_t|}{2}\right),$$

ϕ = MV init cond * NLO BK evolution
or some parametrization (Kharzeev-Kovchegov-Tuchin)

e.g., $T_{q\bar{q}}(rQ_s,x) = 1-\exp\left[-(rQ_s)^{2\gamma(rQs,x)}/4\right]$

$$2\gamma(rQs,x)-1 = \frac{|\ln[(rQ_s)^2]|}{|\ln[(rQ_s)^2]| + d\sqrt{|\ln[(rQ_s)^2]|\ln(1/x)} + \lambda\ln(1/x)}$$

Implications to HIC phenomenology

NLO-BK Albacete (2007)

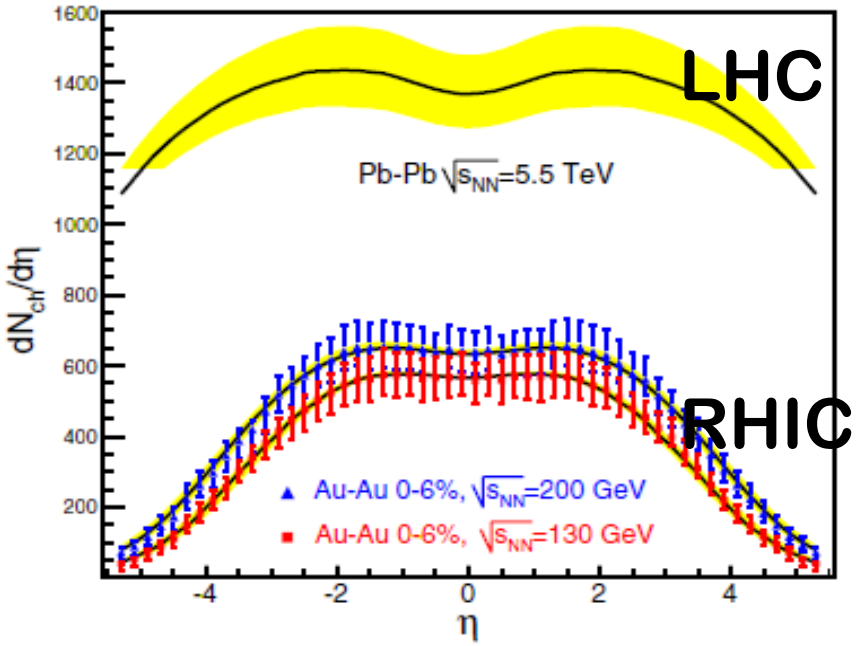

FIG. 2 (color online). Pseudorapidity density of charged particles produced in Au-Au 0%–6% central collisions at $\sqrt{s_{NN}} =$ 130 and 200 GeV and for Pb-Pb central collisions at $\sqrt{s_{NN}} =$ 5.5 TeV. Data taken from [6]. The upper, central (solid lines), and lower limits of the theoretical uncertainty band correspond to ($Q_0 = 1$ GeV, $\Delta Y = 1$), ($Q_0 = 0.75$ GeV, $\Delta Y = 3$), and ($Q_0 = 1.25$ GeV, $\Delta Y = 0.5$), respectively, with $m =$ 0.25 GeV in all cases.

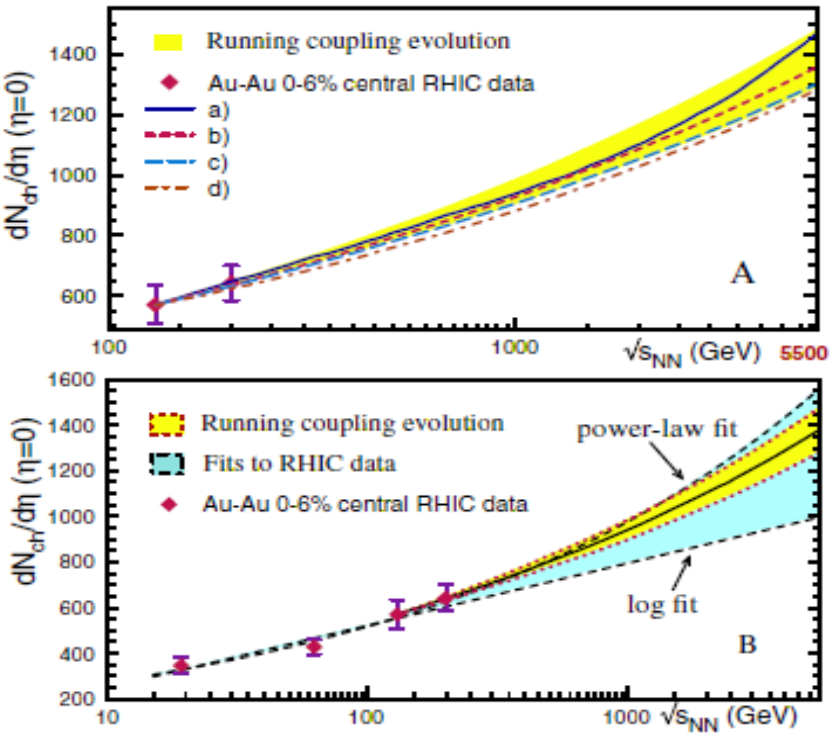

FIG. 3 (color online). Charged particle multiplicity in central Au-Au collisions at $\eta = 0$ versus collision energy. *Upper plot:* Results obtained with the setup leading to Eq. (5) (band) and several modifications of it (see text). *Lower plot:* Power-law, $a\sqrt{s}b$, and logarithmic, $a + b\ln s$, fits to RHIC data at $\sqrt{s_{NN}} =$ 19.2, 64.2, 130, and 200 GeV.

Implications to HIC phenomenology

- **dA での前方抑制 (KKT parametrization)**
  - 核のほうが、飽和効果を早く現す
  - d に比べて抑制

Kharzeev-Kovchegov-Tuchin

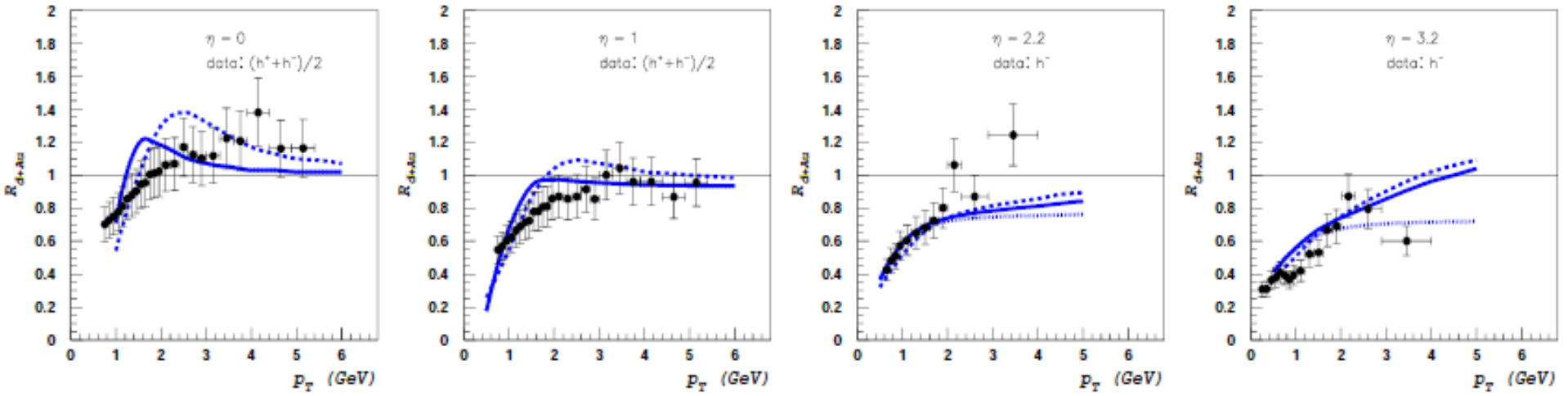

Implications to HIC phenomenology

- dA での pT 依存性（w/ K(eta)）
  - A: 飽和効果のあるモデル（KKT)
  - d; DGLAP

Dumitru-Hayashigaki-JalilianMarian

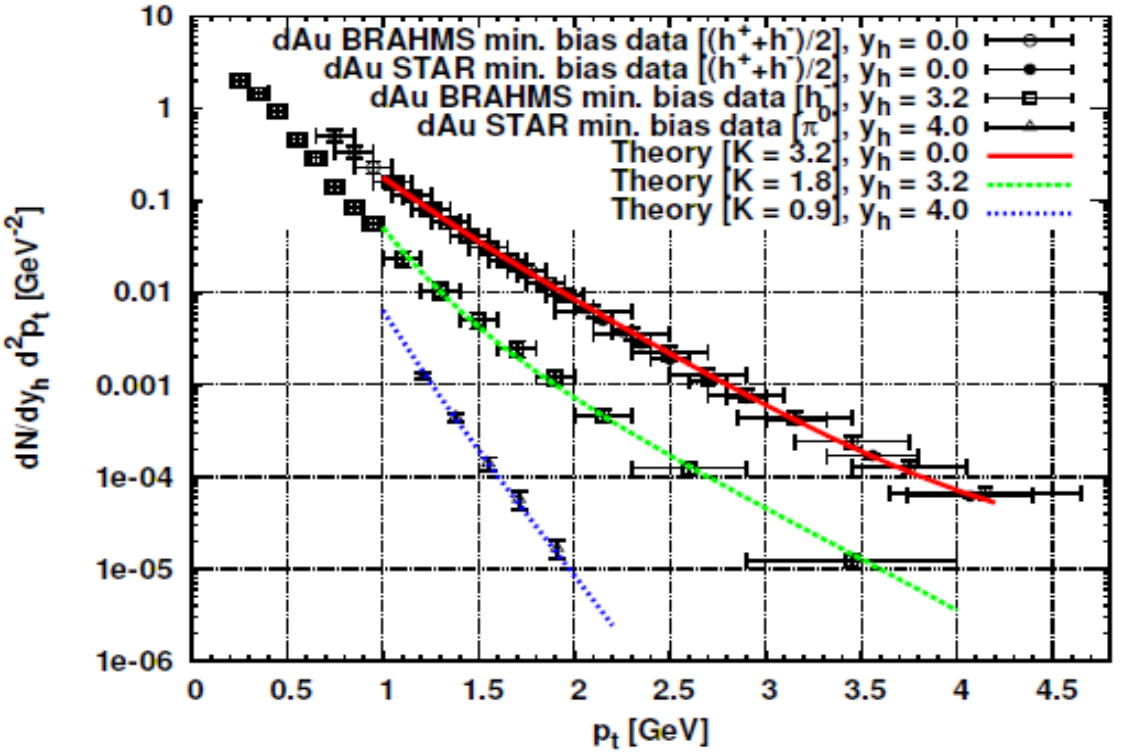

X-evolution for HIC まとめ

- **RHIC データの一側面を捉えている**
  - LO の現象論的モデル
  - Λ_{QCD} < pT < Qs ~ 1GeV が対象
  - 生成粒子相関（方位角相関、峰構造）などの考察が進められている
- **LHC こそ x-evolution の効果大**
  - NLO の記述の重要性 (NLO-BK available)
  - Qs > mc ==> “hard” process への影響
  - pp でも？

Lappi-McLerran

Dense parton dynamics: Glasma

HF-Itakura-Iwazaki

- **RHIC 解析では 1fm/c で熱平衡プラズマを仮定？ how?**
- **CGC は衝突直後の濃密なグルオン場の初期条件を決める**
- 模型化：重イオン衝突＝ **MV** 模型の古典場の時間発展
  - 境界条件

Kovner-Weigert-McLerran

$$\alpha(\tau=0,x_\perp) = -\frac{ig}{2}[\alpha_1^i(x_\perp),\alpha_2^i(x_\perp)],$$
$$\alpha^i(\tau=0,x_\perp) = \alpha_1^i(x_\perp)+\alpha_2^i(x_\perp),$$

$$A_\eta = \mathcal{A}_\eta = -\tau^2\alpha(\tau,x_\perp), \quad A_i = \mathcal{A}_i = \alpha_i(\tau,x_\perp).$$

T. Lappi's fig.

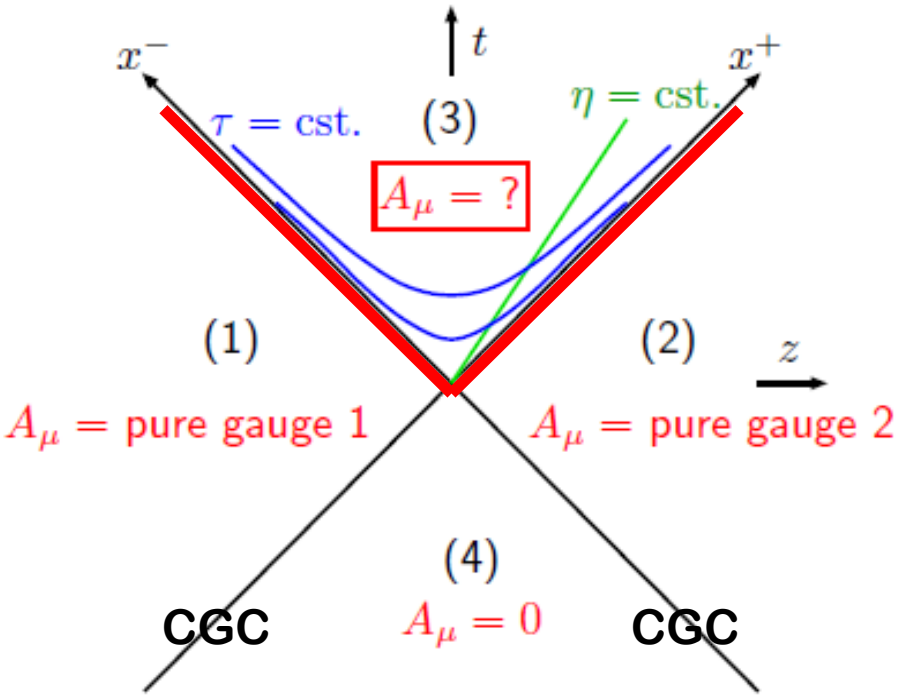

Dense parton dynamics: Glasma

- 衝突直後の場

$$E^z|_{\tau=0+} = -ig[\alpha_1^i, \alpha_2^i],$$
$$B^z|_{\tau=0+} = ig\epsilon_{ij}[\alpha_1^i, \alpha_2^j]$$

- 縦ブースト不変な、カラー電場、磁場縦成分が特徴

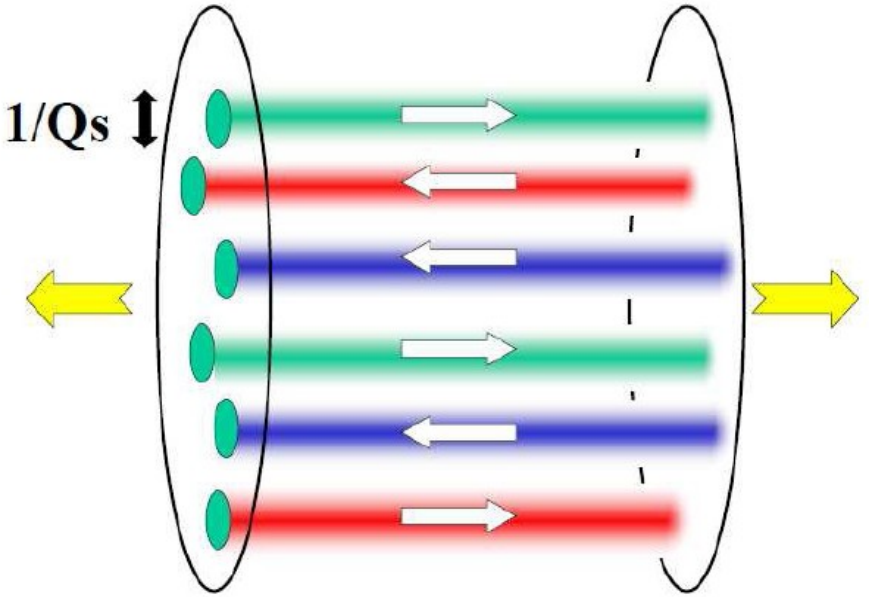

Numerical simulation

T. Lappi (after ensemble average)

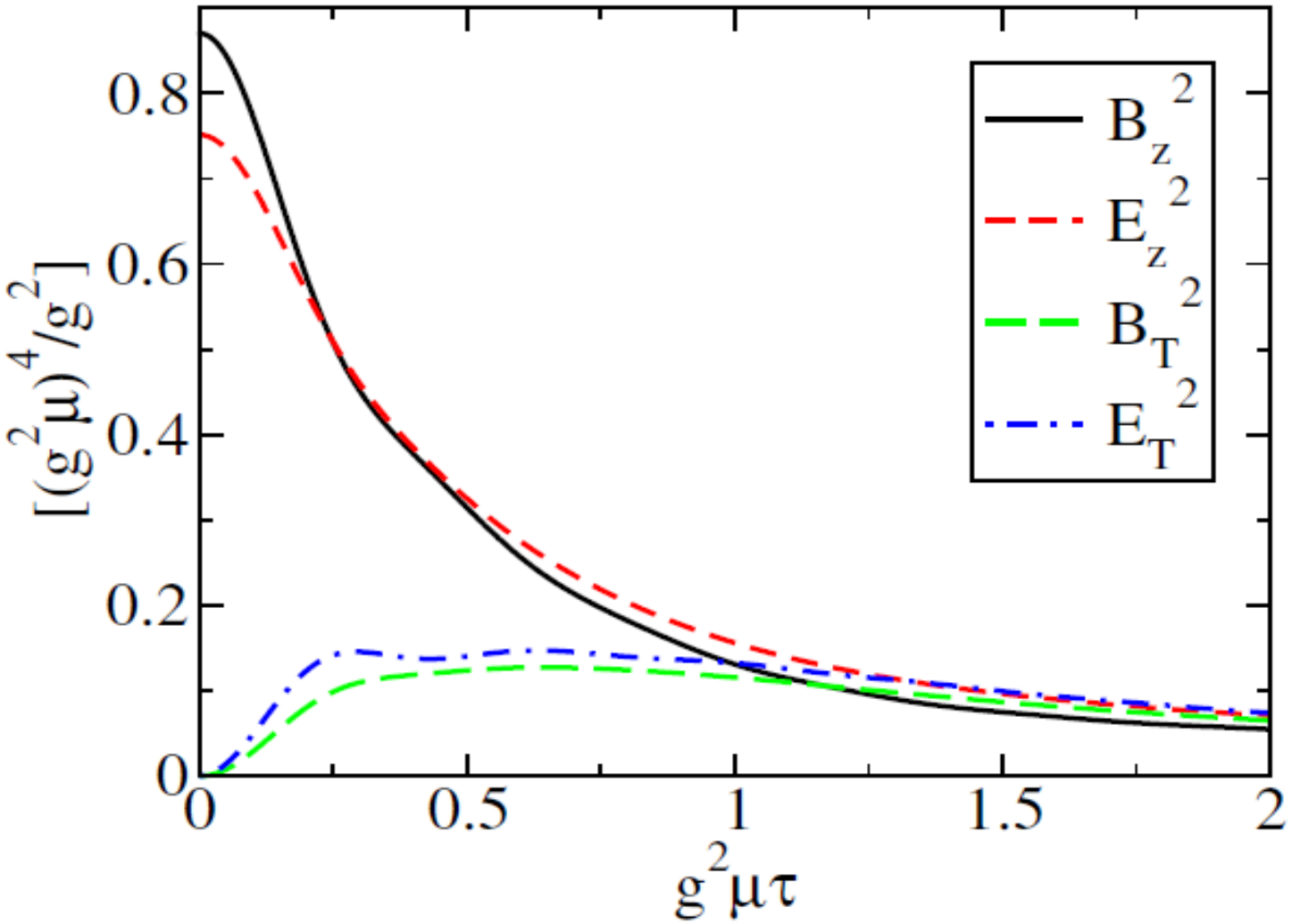

Toward thermalization

- 数値計算と対比して解析的に理解したい
- CGC のアンサンブル平均＝イベント平均
- ブースト不変な背景場だけでは熱化しない
  - 不安定モードによる熱化（もしあれば）は全ての事象に
- 一つのカラー配位に着目
- SU(2) 模型

- 不安定性を数値計算が示唆

Romatschke-Venugopalan

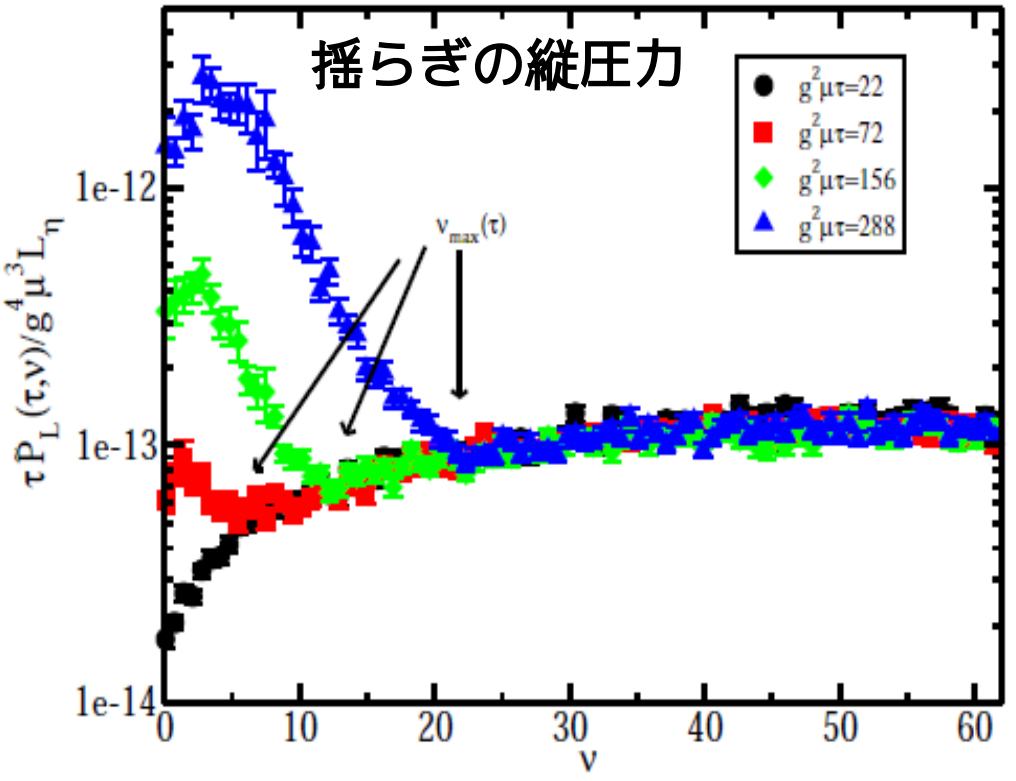

Classical field time-evolution

- 第３方向を向く縦磁場チューブを **exp(-Qs^{2}r^2)** で準備（アベーリアン！） **==>** 解）変形ベッセル関数

■ $Q_s\tau$=0, 0.5, 1.0, 1.5, 2.0

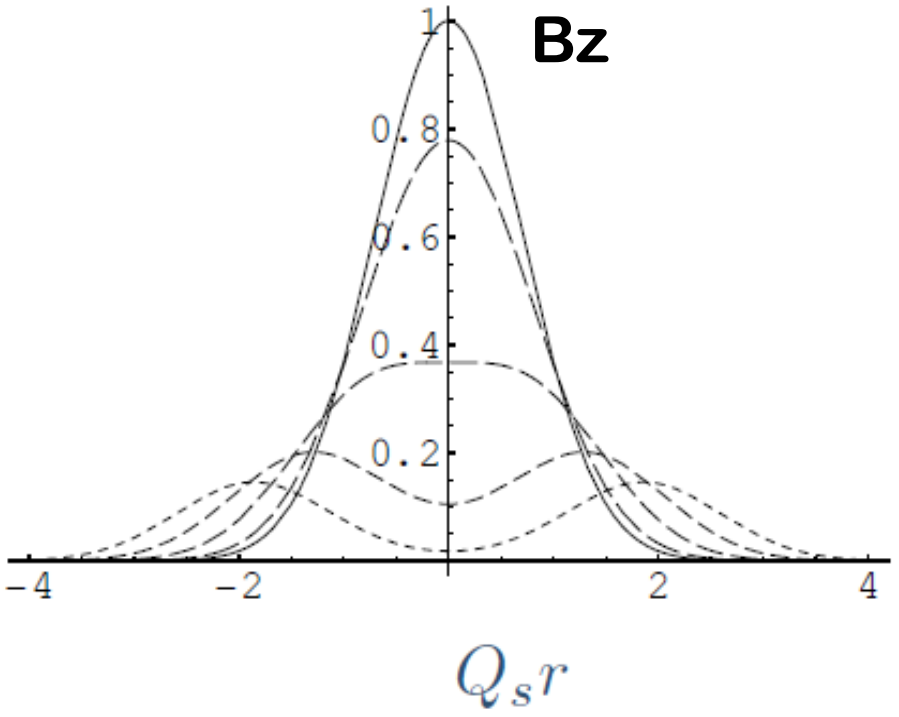

At constant time, $Q_s t = 1, 2$

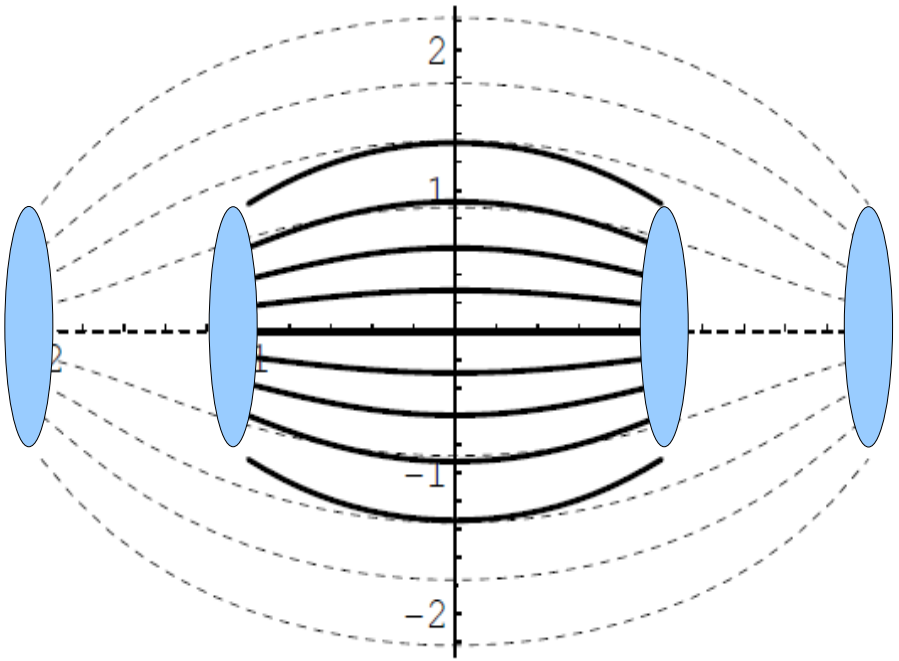

Classical field time-evolution

- エネルギー密度

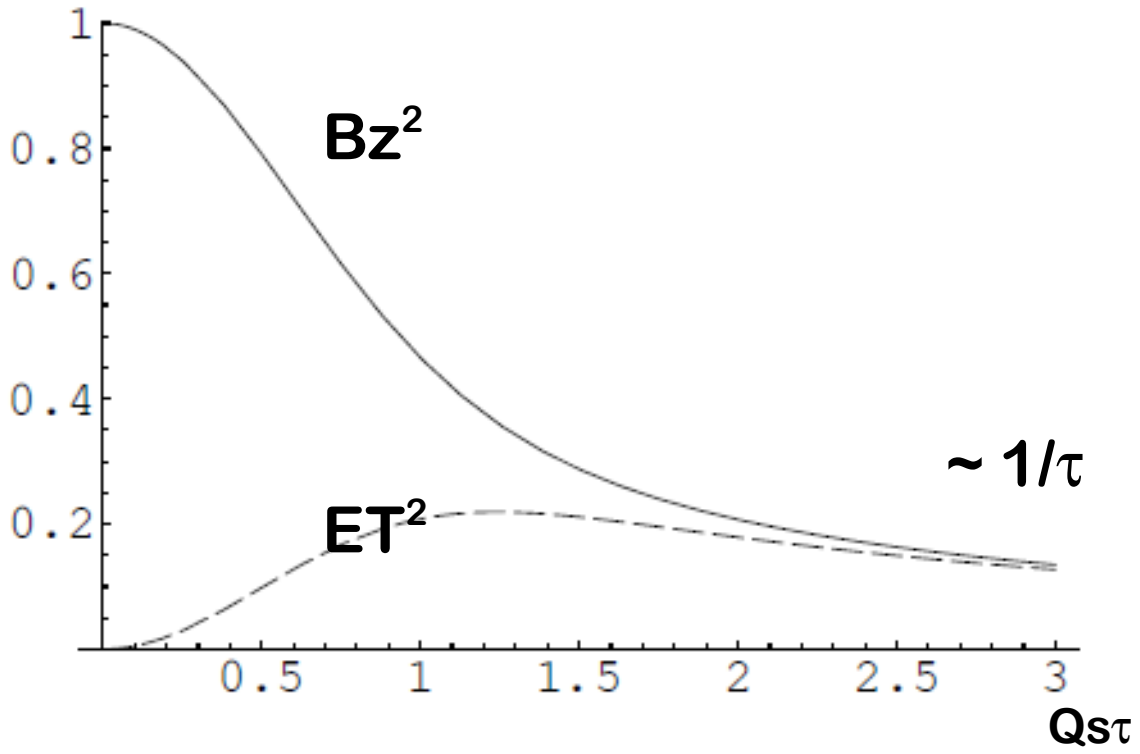

Quite similar to Lappi's: important dynamics is Abelian!??

Long. pressure is negative: $(\overline{(B^z)^2} - \overline{(E^T)^2})/2$

Fluctuations around Classical field

- 古典解まわりの揺らぎの安定性解析

$$A_i = \mathcal{A}_i + a_i(\tau, \eta, x_\perp)\,, \quad A_\eta = \mathcal{A}_\eta + a_\eta(\tau, \eta, x_\perp)$$

- 簡単のため、一定古典場の場合

$$\alpha = 0, \qquad \alpha_i^a = \delta^{a3}\frac{B}{2}\left(y\delta_{i1} - x\delta_{i2}\right)$$

- **Spin-B coupling --> Nielsen-Olesen 不安定性**

$$\frac{1}{\tau}\partial_\tau(\tau\partial_\tau\tilde{a}_+^{(\pm)}) + \left(E_n \mp mgB \pm 2gB + \frac{\nu^2}{\tau^2}\right)\tilde{a}_+^{(\pm)} = 0$$

Landau level

rapidity-mom.

Fluctuations around Classical field

- **For lowest Landau level**

$$\partial_\tau^2 f + \frac{1}{\tau}\partial_\tau f + \left(-gB + \frac{\nu^2}{\tau^2}\right) f = 0$$

- 時間とともにバネ定数が零、負に

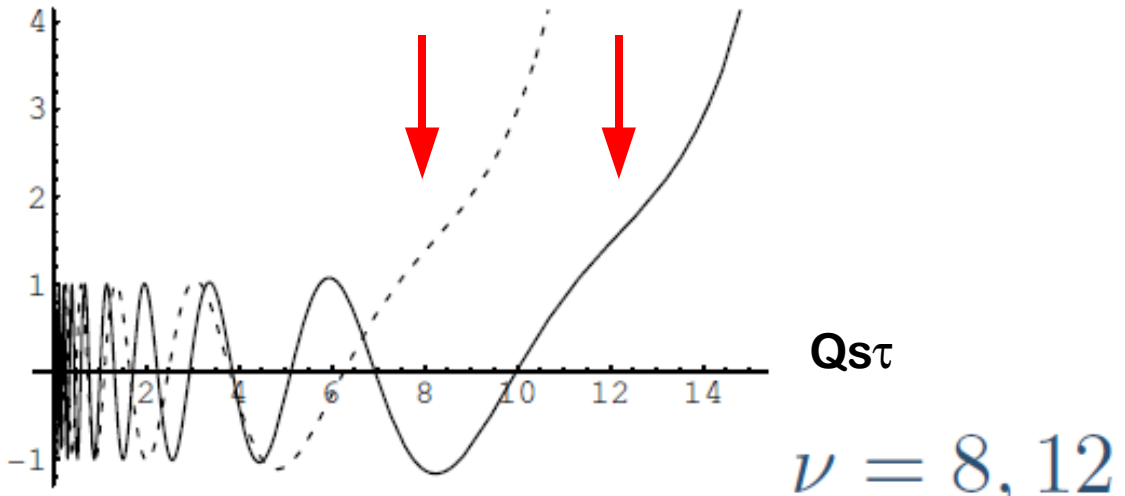

Numerical simulation II

- $\nu \sim \tau$ is observed

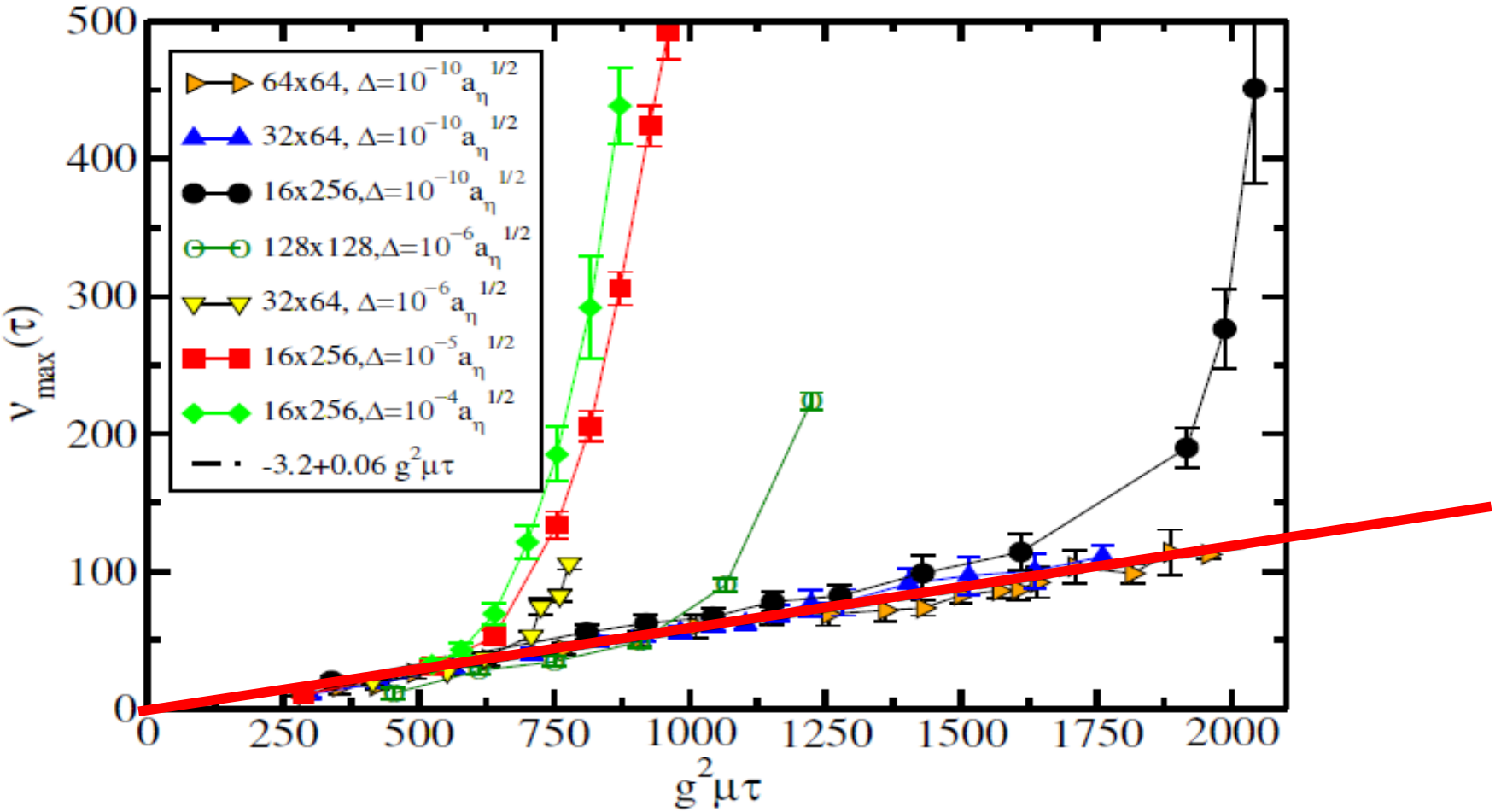

Glasma　まとめ

- ブースト不変な古典場の数値計算をアーベリアンなフラックスチューブが再現した。
  - 非可換性の役割は？

- 古典磁場まわりの不安定揺らぎ（**NO** タイプ）は、数値計算と同様の振舞いをもつ。
  - 電場の場合の不安定性は？
  - 電場磁場の共存する場合は？
  - **SU(3)** の場合は？
  - **Weibel** 不安定性との関連は？